*Journal of the European Ceramic Society* **19** (1999) 1665–1673

PII: S0955-2219(98)00263-5
0955-2219/99/$ - see front matter

# Synthesis and Characterisation of $La_{0.95}Sr_{0.05}GaO_{3-\delta}$, $La_{0.95}Sr_{0.05}AlO_{3-\delta}$ and $Y_{0.95}Sr_{0.05}AlO_{3-\delta}$

P. S. Anderson,[a] G. C. Mather,[b] F. M. B. Marques,[b]* D. C. Sinclair[a] and A. R. West[a]

[a]Chemistry Department, University of Aberdeen, Aberdeen AB24 3UE, UK
[b]Ceramics and Glass Engineering Department, UIMC, University of Aveiro, 3810 Aveiro, Portugal

(Received 3 August 1998; accepted 26 October 1998)

***Abstract***

*The oxide-ion conducting phases $La_{0.95}Sr_{0.05}GaO_{3-\delta}$ (LSG), $La_{0.95}Sr_{0.05}AlO_{3-\delta}$ (LSA) and $Y_{0.95}Sr_{0.05}AlO_{3-\delta}$ (YSA) have been synthesised, either by solid state reaction or through a chemical route. Structural and microstructural characterisation was carried out using XRD and SEM/EDS techniques and a.c. impedance spectroscopy (250–1000°C) was employed to determine the electrical properties. Although low-temperature impedance results were strongly dependent on phase purity and microstructure, high temperature electrical conductivity data could be used to compare the electrical conductivities of LSG, LSA and YSA. Chemical modification from the well-known Sr-doped lanthanum gallate via replacement of different cations on the A and/or B site decreased the conductivity, increased the activation energies and decreased the ionic conductivities. From the results, there is no simple correlation between oxygen ion conductivity and geometric aspects related to unit cell parameters and cation radii. Instead, cation polarisability seems to play an extremely important role in designing improved oxygen ion conductors based on the perovskite structure.* © *1999 Elsevier Science Limited. All rights reserved*

*Keywords*: electrical properties, perovskites, microstructure: final, lanthanum gallate, ionic conductivity.

## 1 Introduction

Potential applications of oxygen ion conductors are numerous, including uses such as components in oxygen sensors, oxygen pumps and oxygen-permeable membranes. They have also been studied for application in solid oxide fuel cells (SOFC), which offer a clean, pollution-free alternative energy source for the electrochemical generation of electricity at high efficiency.

The most widely researched oxide ion conductors are those with the fluorite structure which contain tetravalent cations, such as zirconium ($ZrO_2$) and cerium ($CeO_2$).[1] Currently, $Y_2O_3$-stabilised $ZrO_2$ (YSZ) is the most common electrolyte used in SOFCs, however, the oxide ion conductivity in YSZ is rather low for fuel cell applications. Due to the low conductivity, SOFCs which use YSZ electrolytes must operate at around 1000°C, which leads to problems associated with high costs and the ability of the materials to function at the operating temperature. In particular, there are problems associated with phase stability of the various component materials and their compatibility at ca 1000°C.

These constraints have led to the investigation of other possible oxide-ion conducting materials, including $ABO_3$ oxides based on the perovskite structure. Perovskites offer numerous advantages, including the stability of the crystal structure, the variety of elements which can be accommodated in the crystal lattice, and the ease with which oxygen vacancies can be produced by partial substitution of the A- and/or B-site cations with lower valence cations. The suitability of a wide range of perovskitic oxides as potential oxide ion conductors have been analysed.[2–7] Recently, $LaGaO_3$-based perovskite-type oxides have been shown to exhibit extremely high oxide-ion conductivity.[2–6] Before this discovery, research into oxide ion conducting perovskite-based materials had led to disappointing results.[7] The $LaGaO_3$-based perovskite-type oxides have ionic transport numbers close to unity,

*To whom correspondence should be addressed. Fax: +351-34-25300; e-mail: fmarques@cv.ua.pt

exhibit large electrolytic domains and are insensitive to moisture, all of which are essential characteristics for an electrolyte material in high-temperature fuel cells.[2–6]

The electrical conductivity of $LaGaO_3$ depends strongly on the alkaline earth cation which is doped on the La site, and increases in the order: Sr > Ba > Ca. A-site doping with a cation of lower oxidation state can lead to a large number of oxide vacancies being formed and, therefore, to an increase in oxide-ion conductivity. The electrical conductivity increases with the level of Sr-doping and reaches a maximum value at $x = 0{\cdot}1$ in $La_{1-x}Sr_xGaO_3$.[5]

The influence of B-site doping on the electrical properties of LSG-based materials has also been studied. The electrical conductivity of $La_{0{\cdot}9}Sr_{0{\cdot}1}GaO_3$ increases with partial substitution of Mg, Al or In for Ga, with Mg producing the largest increase in the conductivity. The solid solution limit and maximum value of oxide ionic conductivity in $La_{0{\cdot}9}Sr_{0{\cdot}1}Ga_{1-y}Mg_yO_3$ was observed for $y = 0{\cdot}2$.[5]

Doped-$LaGaO_3$ materials are promising oxide ionic conductors, with conductivity values higher than that of the fluorite-type $ZrO_2$- or $CeO_2$-based materials. However, there are problems associated with using LSG-based materials as solid electrolytes in SOFCs. In particular, the high cost of gallium compounds and their low mechanical strength, especially at fuel cell operating temperatures, means that replacement of Ga in these materials is highly desirable.

In this paper, we describe the synthesis of $La_{0{\cdot}95}Sr_{0{\cdot}05}GaO_{3-\delta}$ (LSG), $La_{0{\cdot}95}Sr_{0{\cdot}05}AlO_{3-\delta}$ (LSA) and $Y_{0{\cdot}95}Sr_{0{\cdot}05}AlO_{3-\delta}$ (YSA), their structural and microstructural characterisation and the measurement of their electrical properties using, for the most part, a.c. impedance spectroscopy in air (250–1000°C). The central objective was to observe the effect, if any, of different A and B site cations on the electrical conductivity of these perovskite-based materials. An A site Sr-doping level of 5% was chosen in order to generate a reasonable concentration of oxygen vacancies and to avoid the formation of secondary phases as the solubility limit of Sr in lanthanum gallate occurs at 10% Sr.[5] The other host cations were chosen in order to, preserve electroneutrality, have similar chemical characteristics (Al and Ga are both in group XIII of the periodic table and $Y^{3+}$ is a common replacement for trivalent rare earth cations such as $La^{3+}$ and $Dy^{3+}$) but have different ionic radii. In order to obtain a comparative analysis of the role of A- and B-site cations on the electrical properties in this series of perovskites, we consider LSA as a reference material; LSG and YSA then provide examples of materials containing larger B-site and smaller A-site cations, respectively.

## 2 Experimental

### 2.1 Sample preparation

LSG was prepared by the conventional ceramic route from appropriate stoichiometric amounts of $La_2O_3$, $SrCO_3$ and $Ga_2O_3$. The reagents were mixed, wet-milled in ethanol with zirconia balls in a Teflon container. The dried mixture was then calcined at 1100°C for 12 h, ball-milled again, dried and screened through a mesh in order to obtain a powder fraction with an average particle size of less than 30 $\mu$m. The powder was pressed into pellets using a 20 mm die and sintered at 1500°C for 4 h in order to obtain dense pellets.

LSA was initially prepared by the conventional ceramic route from stoichiometric amounts of the reagents $La_2O_3$, $SrCO_3$ and $Al_2O_3$. The experimental procedure was the same as described for the LSG sample, but due to incomplete reaction at 1500°C, sintering was repeated at 1675°C for a further 4 h. As the sintered pellets were of low density, an alternative synthetic route via a chemical precipitation method was employed in an attempt to obtain higher surface area powders which could then be sintered into high density ceramics.

The chemical precipitation route involved preparing solutions of $La^{3+}$ and $Al^{3+}$ (of known concentrations) from the addition of HCl to $La_2O_3$ and $Al(OH)_3$, respectively. The precipitation method involved mixing the metal cations in appropriate stoichiometric proportions, followed by addition of $NH_4OH$ solution, in order to obtain the $La(OH)_3$ and $Al(OH)_3$ precipitates with mixing on a micron scale. This precipitate was filtered, washed and dried overnight at 60°C, ball-milled with a stoichiometric amount of $SrCO_3$, then dried and calcined at 1100°C for 12 h. The mixture was then ball-milled again, screened through a 30 $\mu$m mesh and pelletised as before; final firing took place at 1700°C for 4 h.

YSA was also initially prepared by the conventional ceramic route using the reagents $Y_2O_3$, $SrCO_3$ and $Al_2O_3$ in stoichiometric proportions. The reagents were mixed, ball-milled and calcined at 1100°C for 12 h but limited reaction had taken place at this temperature, so the mixture was refired at 1500°C for 12 h. Considering the excessively high temperature required to achieve reaction between precursors, sintering of these powders to produce dense pellets was difficult; YSA was, therefore, also prepared by the chemical precipitation route.

The chemical precipitation route involved using $YCl_3$ and the previously prepared $Al^{3+}$ solution in appropriate stoichiometric proportions. The solutions were mixed as before and excess $NH_4OH$ solution was added to raise the pH in order to obtain a precipitate of $Y(OH)_3$ and $Al(OH)_3$. This precipitate was treated in the same manner as the chemically prepared LSA sample, with unreacted pellets fired at 1700°C for 4 h.

Characterisation of samples initially involved XRD analysis of both calcined and sintered materials, over a 2Θ range from ca 0–80°. Further characterisation was obtained from SEM and EDS analysis, which were used to determine the degree of homogeneity, average grain size and porosity of the samples. Samples for SEM and EDS analysis were polished with diamond paste (7 $\mu$m) and thermally etched by heating to 90% of their sintering temperature for 30 min. All samples were carbon coated prior to SEM and EDS analyses.

Electrical measurements were carried out by a.c. impedance spectroscopy in air with an HP 4284A impedance analyser over a frequency range of 20 to $10^6$ Hz. Measurements were recorded over a temperature range of 250–1000°C, with readings taken every 50°C at temperatures below 500°C and every 100°C above 500°C. Measurements were taken 1 h after changing the furnace temperature, to ensure the samples had attained thermal equilibrium. Complementary electrochemical measurements (conductivity versus oxygen partial pressure and ion-blocking) were also performed to separate ionic and electronic conductivities. Details on the latter measurements are presented elsewhere.[8]

Samples for electrical measurements were prepared by polishing pellets with a series of increasing finer grade SiC grinding papers, before the application of platinum paste to pellet surfaces. Platinum paste (approximately 5 mm in diameter) was applied to the centres of both major faces of the pellets before being fired at 1000°C to remove all organic matter.

## 3 Results and Discussion

### 3.1 Sample characterisation

The XRD powder pattern of LSG, shown in Fig. 1(a), indicated that the phase has the $GdFeO_3$-type orthorhombic perovskite structure, isostructural with $LaGaO_3$ (I.C.D.D. no. 24-1102). A small amount of unidentified impurity phase was present (< 5%). Rietveld refinement of the crystal structure of the orthorhombic phase in S.G. Pnma with the program FULLPROF[9] gave the following unit cell: $a = 5{\cdot}5225(6)$, $b = 7{\cdot}7683(5)$, $c = 5{\cdot}4589(9)$ Å (unit cell parameters for all phases are presented in Table 1. LSG pellets were mechanically strong and dense, with a density value of over 94% of the theoretical density. SEM analysis confirmed the high density of the sample, and indicated a uniform composition and grain size, with an average grain diameter of around 1 $\mu$m (Fig. 2). EDS analysis indicated that the chemical composition was close to that of the desired phase.

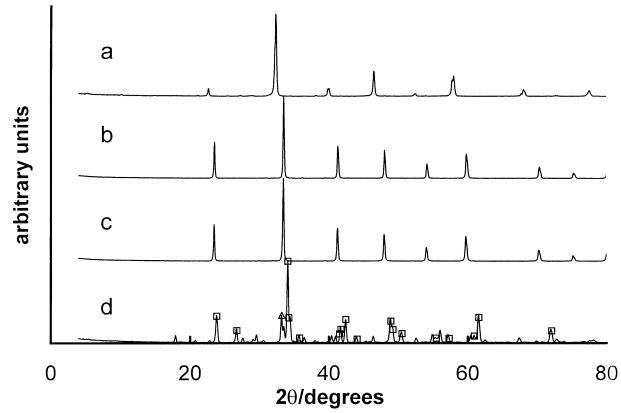


**Fig. 1.** XRD powder diffraction patterns of (a) LSG (ceramic route), (b) LSA (chemical route), (c) LSA (ceramic route), (d) YSA. (chemical route)—the perovskite peaks are identified with the mark □ and the major garnet peak is marked with a △.

The LSA samples prepared by both chemical and ceramic routes have simple cubic perovskite structures (S.G. Pm3m). Refinement of the structure by the Rietveld method indicates that, within the e.s.d. limits, the magnitude of the unit cells prepared by chemical and ceramic methods are equivalent: 3·7914(4) and 3·7915(4) Å, respectively [Fig. 1(b) and Fig. 1(c)] LSA samples prepared by the conventional ceramic route were of low density, around 77% of the theoretical density, whilst those prepared by the chemical route had greater mechanical strength and density, over 89% of the theoretical density. Although XRD indicated that LSA prepared by the two methods have identical structures, SEM and EDS analyses indicated that there were large differences in microstructure between the two samples. The sample prepared by the ceramic route was confirmed to be a highly porous, fine grained material, with an average grain size of less than 1 $\mu$m (Fig. 3). SEM analysis indicated that the material was single phase, whilst the EDS analysis indicated that the chemical composition was close to that of the desired phase.

In contrast, SEM and EDS analyses of the phase prepared by the chemical route indicated the presence of three phases (Fig. 4). SEM analysis revealed a dense sample, composed of two phases with large grains and a third phase with a fine grain matrix. EDS analysis indicated that the large, dark grains (grain A, Fig. 4) were extremely rich in Al (ca 88 atm%), with a low La content (ca 9 atm%)

**Table 1.** Phase identification and cell parameters for LSG, LSA and YSA

| *Nominal compositions* | $La_{0.95}Sr_{0.05}GaO_{3-\delta}$ (ceramic) | $La_{0.95}Sr_{0.05}AlO_{3-\delta}$ (ceramic) | $Y_{0.95}Sr_{0.05}AlO_{3-\delta}$ (chemical) |
|---|---|---|---|
| Major phase | Perovskite | Perovskite | Perovskite |
| Symmetry | Orthorhombic | Cubic | Orthorhombic |
| Lattice parameters (Å) | $a = 5{\cdot}5225(6)$<br>$b = 7{\cdot}7683(5)$<br>$c = 5{\cdot}4589(9)$ | $a = 3{\cdot}7915(4)$[a] | $a = 5{\cdot}328(7)$<br>$b = 7{\cdot}417(9)$<br>$c = 5{\cdot}208(6)$ |
| Unit cell volume (Å$^3$) | 234·19(2) | 54·51(1) | 205·81(6) |
| Theoretical Density[b] (g cm$^3$) | 7.19(1) | 6.42(3) | 5.25(2) |
| Equivalent 'cubic' lattice parameter (Å) | 3·9000 | 3·7915 | 3·719 |
| Secondary phase | Unidentified | Unidentified | Cubic garnet |

[a]A similar value was found for the chemically processed LSA [$a = 3{\cdot}7914(4)$ Å].
[b]Assuming the nominal compositions and that Sr in the A-site is compensated by oxygen vacancies, i.e. $[Sr_{La}'] = 2\,[V_o^{\bullet\bullet}]$.
[c]To estimate the critical radius shown in Table 2. For orthorhombic symmetry, the equivalent 'cubic' parameter ('$a$') was estimated by calculating the volume ($V$) which one perovskite formula unit would occupy in the orthorhombic unit cell ('$a$' $= V^{1/3}$).

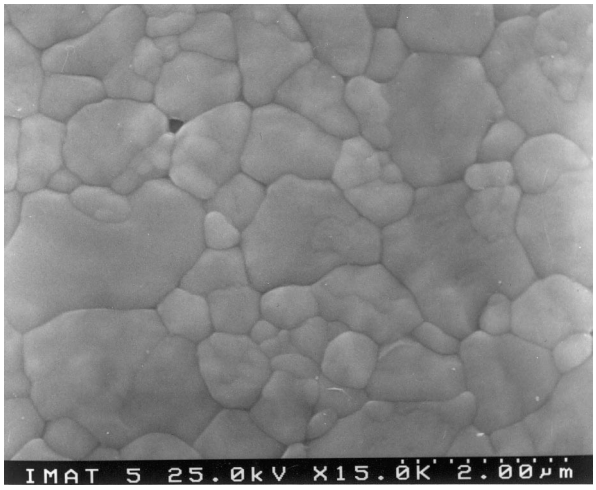


**Fig. 2.** Scanning electron micrograph of polished and thermally etched surfaces of LSG.


**Fig. 3.** Scanning electron micrograph of polished and thermally etched surfaces of LSA (ceramic method).

and a significant level of Sr (ca 3 atm%). The large lighter grains (grain B, Fig. 4) were found to contain a high level of La (ca 64 atm%) with a lower level of Al (ca 36 atm%), and virtually no Sr (ca 0.3 atm%). The finer grained matrix (grain C, Fig. 4) had a composition close to that of the desired phase, but with slightly less Sr than expected. The grain size of the main phase (fine grained matrix) was ca 2–3 $\mu$m and therefore slightly larger than that of the LSA prepared via the mixed oxide route.

The refractory nature of the reagents made it difficult to achieve phase purity and to sinter dense pellets of LSA via the mixed oxide route. Failure to produce single phase materials from the chemical precipitation route was probably associated with the poor control of the stoichiometry of the precursor $La(OH)_3$–$Al(OH)_3$ powder. In order to try and produce phase-pure, chemically precipitated LSA material, the preparation route was altered slightly; a solution of $LaCl_3$ and $AlCl_3$ was added to an excess of $NH_4OH$, rather than adding the $NH_4OH$ to the chloride solution. This method was employed in order to prevent problems associated with the pH slowly increasing as the $NH_4OH$ was added, thus avoiding problems associated with the precipitation of $La^{3+}$ and $Al^{3+}$ at different pH values. a.c. impedance measurements on this LSA sample showed similar behaviour to the LSA samples prepared via the other routes.

The XRD powder pattern of YSA, Fig. 1(d), indicated the presence of two phases: the orthorhombic $GdFeO_3$-type perovskite structure (I.C.D.D. no. 34-41) and a cubic phase of similar composition with the garnet structure (I.C.D.D. no. 38-222). Reflections from the perovskite phase are indicated in Fig. 1. Refinement of the more dominant orthorhombic phase gave the following unit cell: $a = 5{\cdot}328(6)$, $b = 7{\cdot}417(9)$, $c = 5{\cdot}208(6)$ Å. The YSA pellets prepared by the chemical precipitation route were mechanically strong and dense. SEM

confirmed the density of the sample, and also revealed the presence of two distinct areas, one of large grain size, and the other a matrix of small grain size (Fig. 5). The larger areas had grain sizes ranging from around 5–20 $\mu$m, whereas the matrix had an average grain size of 2–3 $\mu$m. EDS analysis indicated that both the large- and small-sized grains had chemical compositions similar to that of the desired phase. The large- and small-grain regions are most likely to be associated with garnet and perovskite forms, respectively, in accordance with the XRD data.

### 3.2 Electrical characterisation

The a.c. impedance data of LSG (see Fig. 6) in air showed two distinct arcs: a small, high frequency arc attributed to the bulk response (associated capacitance value around $10^{-12}$ F) and a larger grain-boundary arc (associated capacitance value $10^{-11}$–$10^{-8}$ F); there was also an electrode spike at low frequencies (associated capacitance value $10^{-7}$–$10^{-5}$ F) which became more apparent with increasing temperature. Bulk and grain boundary conductivities as a function of temperature are shown in the form of an Arrhenius plot (Fig. 7). Activation energies for each component were calculated from the Arrhenius plots at both high and low temperatures.

The bulk activation energy ($E_a$) is usually the sum of a migration enthalpy ($\Delta H_m$) and an association enthalpy ($\Delta H_a$) term. At low temperatures, both are present, but with increasing temperature the Coulombic forces between positive (oxygen vacancies) and negative defects (A-site dopant) decrease due to increased thermal energy, leaving only $\Delta H_m$ at elevated temperatures.[10] The obvious change in slope between the low temperature bulk conductivity ($E_a = 72{\cdot}4$ kJ mol$^{-1}$) and the high temperature total conductivity (governed by the bulk transport, with $\Delta H_m = 60.3$ kJ mol$^{-1}$) is consistent with this general trend (Fig. 7), and provides an estimate for the association enthalpy ($\Delta H_a$) of 12·1 kJ mol$^{-1}$. For 10% Sr-doped LSG, similar values were reported for the high temperature migration enthalpy (55·0 kJ mol$^{-1}$) and low temperature bulk conductivity (66·6 kJ mol$^{-1}$.[11] Overall, the association enthalpies are small in both cases and similar (or even lower) than those reported for oxides with the fluorite-type structure.[10]

The resistive nature of the grain boundary, with a high activation energy (ca 90 kJ/mol$^{-1}$), prevents the material exhibiting the high conductivity associated with the bulk response. This highly resistive grain boundary response has been attributed to the formation of a Sr-rich liquid phase which forms during high temperature sintering[11] and is located at the grain boundaries.

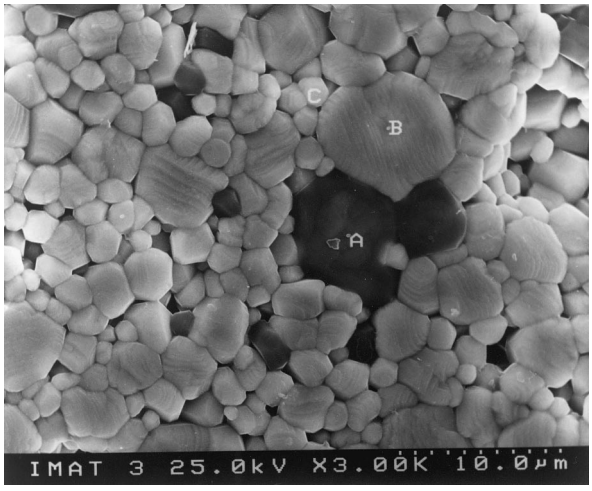


**Fig. 4.** Scanning electron micrograph of polished and thermally etched surfaces of LSA (chemical method).

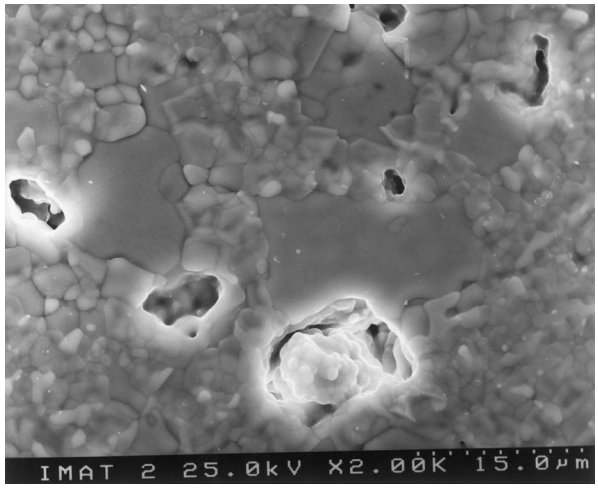


**Fig. 5.** Scanning electron micrograph of polished and thermally etched surfaces of YSA (chemical method).

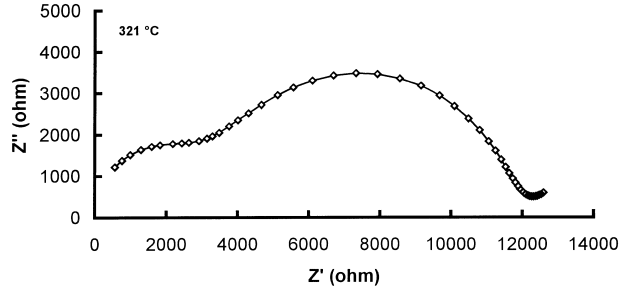


**Fig. 6.** Impedance spectrum of LSG (ceramic method), in air.

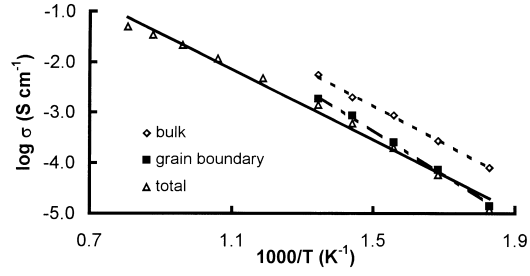


**Fig. 7.** Arrhenius plots of total, bulk and grain boundary conductivities of LSG.

Impedance analysis was carried out on LSA pellets prepared by both the ceramic and chemical precipitation routes. The ceramic LSA was found to be more resistive than the LSG sample (Fig. 8), with only one discernible arc present in the impedance plots with an associated capacitance value of around $10^{-10}$ F. This behaviour is typical of a poorly sintered ceramic. The porosity (slightly higher than 20%) can also account for a relatively small drop in conductivity with respect to a dense pellet. In the case of zirconia-based electrolytes, an approximate relationship is observed between porosity (up to ca 30% porosity) and a decrease in conductivity. For every 10% increase in porosity, a drop in bulk conductivity of about 20% (from the value observed for the fully dense material) is observed.[12] This observation is relevant to the conductivity values observed for the materials under study because although the conductivities of LSA are more than one order of magnitude lower than for LSG, such large differences in conductivity cannot be rationalised only by sample porosity.

The LSA samples prepared via chemical precipitation were observed to be very resistive materials, with a single, large arc only becoming apparent around 500°C. The arc had an associated capacitance value of around $10^{-9}$ F. The relaxation frequency of this arc was different to that observed for LSA samples prepared via the mixed oxide route. The presence of secondary phases in these samples is likely to have a considerable effect on the measured electrical properties, especially at low temperatures. Due to the poor quality and inhomogeneous nature of the LSA samples prepared via the precipitation route, all subsequent measurements for LSA materials relate to the samples prepared via the mixed oxide route.

Impedance analysis of YSA indicated that these samples were the most resistive of all the materials studied (Fig. 9) with a single, large unsymmetrical arc only appearing at temperatures above 600°C. This arc is likely to be a complex combination of the bulk and grain boundary responses, together with a composite effect due to the presence of the garnet phase. The presence of insulating phases dispersed in a solid electrolyte is known to be able to change dramatically the shape of the complex impedance plane plots due to ion-blocking effects associated with the dispersed phase.[13] No attempt was made to resolve this arc into different contributions. However, as the perovskite was the dominant phase and the garnet a dispersed phase, the general behaviour of the sample is believed to be governed by the perovskite phase, albeit with conductivity values which might be lower than for the pure perovskite. Comments similar to those already made for the LSA samples concerning the role of porosity are also relevant in this case, based on the known role of insulating phases (e.g. alumina) dispersed in solid electrolytes (e.g. yttria stabilised zirconia).[13] A small arc with an associated capacitance of ca $10^{-7}$ F was also present at low frequencies, and was attributed to an ion blocking, electrode response.

The conductivities obtained from the LSA and YSA impedance plots were used to produce Arrhenius plots from which activation energies were calculated. The values were higher than for LSG, and the conductivities were lower. As mentioned previously, in doped non-stoichiometric oxides, defect association commonly takes place between the dopant cations and the compensating oxygen vacancies. Due to the difficulty in separating bulk and total conductivities at low temperatures, association enthalpies in LSA or YSA could not be estimated from the data. Improved processing routes leading to better microstructures may provide better quality ceramics from which data on the correlation between ion size and association enthalpies in these families of materials can be obtained. Considering the problems encountered in the preliminary characterisation of the different samples, only the electrical properties of two samples prepared by the ceramic route (LSG and LSA) and one chemically prepared sample (YSA) are considered in the following discussion.

Although the total conductivity could be determined from the impedance spectra, it was not possible to separate the ionic and electronic conductivities in these materials via impedance spectroscopy measurements conducted in air. This

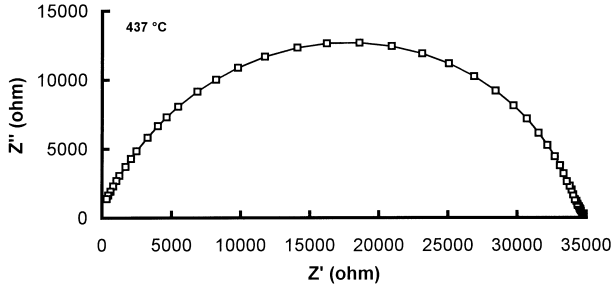


**Fig. 8.** Impedance spectrum of LSA (ceramic method), in air.

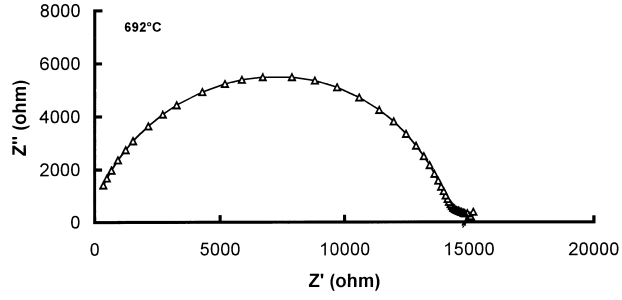


**Fig. 9.** Impedance spectrum of YSA (chemical method), in air.

is often a major problem when attempting to correlate the structural characteristics of these materials with their electrical properties. An associated problem is that this lack of information makes it more difficult to identify relevant criteria which may be of use when designing new solid electrolytes with the perovskite structure.

In order to obtain more information on the ionic and electronic conductivity of these materials, a detailed additional electrochemical characterisation was carried out.

This consisted of high-temperature constant-frequency (10 kHz) conductivity measurements as a function of oxygen partial pressure and ion-blocking measurements.[14] The value of these techniques in determining mixed conduction in similar systems is well documented.[8,15] The former technique usually provides enough information to separate ionic from electronic contributions when the ionic transport number is clearly lower than unity. The appropriateness of these constant frequency measurements has already been demonstrated for a variety of materials,[8,15] and was checked in the present study. Ion-blocking measurements are, on the other hand, especially useful for electrolytes with only minor electronic conductivities.[8,15]

A typical set of results obtained for constant frequency measurements at 900°C is shown in Fig. 10. Separation of ionic from electronic conductivity contributions was easily performed in the case of LSA and YSA because of the dominance of ionic conductivity under reducing conditions (almost constant conductivity) and the clear onset of p-type conductivity in more oxidising conditions. The flatness of the LSG curves justified the need for the ion-blocking technique. Details of the experimental results and procedure adopted in the treatment of these data are described elsewhere.[14] A summary of relevant data necessary for the following discussion is shown in Table 2.

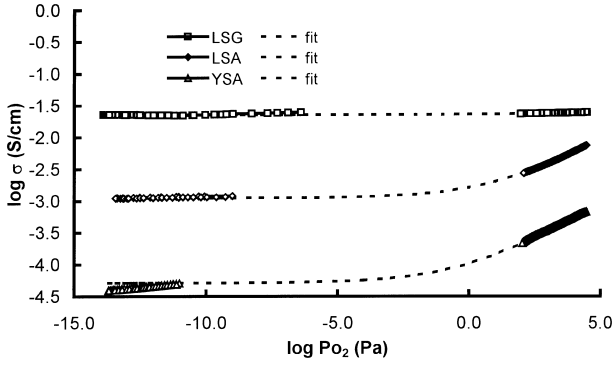


**Fig. 10.** Conductivity versus $Po_2$ for LSG, LSA and YSA, at 900°C. The dashed lines correspond to the best fit to a model behaviour where the ionic conductivity is assumed constant and the p-type conductivity proportional to $Po_2^{1/4}$. Ionic conductivities and activation energies (800–1000°C) obtained from this fitting are shown in Table 2.

**Table 2.** Critical radii, ionic conductivies (at 1000°C) and activation energies

| | *Critical radius* ($r_{crit}$) (Å) | *Ionic conductivity* ($S\,cm^{-1}$) | *Migration enthalpy* ($kJ\,mol^{-1}$) |
|---|---|---|---|
| LSG | 0·7511 | $3{\cdot}6\times10^{-2}$ | 60·3 |
| LSA | 0·9028 | $2{\cdot}4\times10^{-3}$ | 111 |
| YSA | 1·0273 | $1{\cdot}4\times10^{-4}$ | 93·6 |

### 3.3 Correlation between structure and ionic conductivity

In perovskite compounds, migration of anions is via a vacancy mechanism that takes place most readily along the ⟨110⟩ edges of the anion octahedra. A parameter, $r_{crit}$, can be calculated, which is the critical radius between two A-site cations and a B-site cation (Fig. 11) through which an anion can pass without disturbing the surrounding cations. Large values of $r_{crit}$ result in less disturbance of the surrounding lattice as the anion migrates through the saddle point, and thus lower the saddle point energy. Using a simple geometric calculation, the value of $r_{crit}$ can be calculated for any perovskite material from the ionic radii and unit cell values. The reported trends are; (a) an increase in B-site cation size increases $r_{crit}$, and (b) a decrease in A-site cation size increases $r_{crit}$. In previous work, $r_{crit}$ has been identified as a relevant parameter to correlate with migration enthalpies.[10]

From the lattice parameters given in Table 1 and reported ionic radii, Table 2, it is possible to correlate the critical radius with the ionic conductivity and activation energy for ionic conduction in LSG, LSA and YSA; details are given in Table 2. Somewhat surprisingly, the ionic conductivity increases with decreasing $r_{crit}$ and the activation energy decreases with decreasing $r_{crit}$. The conclusions extracted from the $r_{crit}$ model are contradictory to

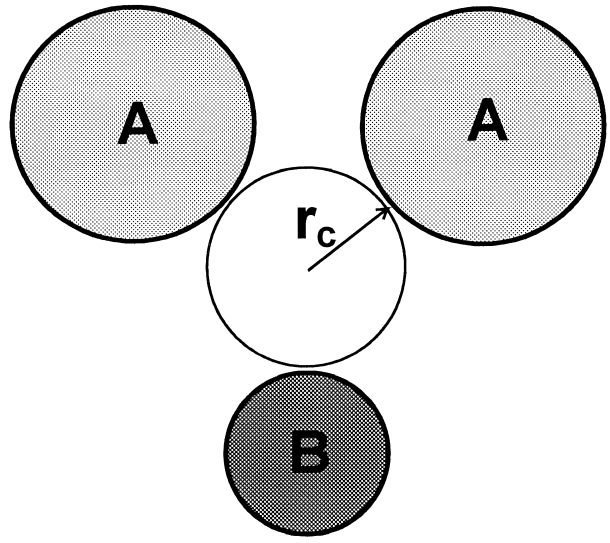


**Fig. 11.** Saddle point configuration showing critical radius ($r_{crit}$) for anion migration in the perovskite structure.

our experimental evidence. The only parameter which may explain such unexpected behaviour is the ionic polarisability of the cations, which was not considered in the original model. We can postulate that small cations act like rigid spheres and the critical radius might be dominant in such circumstances. However, large cations with large polarisabilities (Table 3) are likely to accommodate the migration of a large anion more easily. Although the relevance of this parameter in determining the performance of solid electrolytes with the perovskite structure had already been pointed out, it was not accounted for in the model.[10] When the $r_{crit}$ model was originally proposed, there was also a lack of experimental results on materials with significantly different and well-defined ionic conductivities and activation energies. This restricted the authors to consider only the influence of ion size on the ionic conductivity in perovskite-based materials. Our results show that the geometric model is an oversimplification and that, other factors such as the polarisability of the ions need to be considered when attempting to develop a model to explain the factors which influence the migration of oxide ions in solid electrolytes.

### 3.4 Final remarks

The major difficulties in the present work are associated with poor microstructure and lack of phase purity in the LSA and YSA samples, respectively. The influence of these factors on the electrical measurements deserve some additional comments.

Impedance spectroscopy can be used to study the total conductivity of a given material, to separate grain boundary from bulk contributions and even to confirm the presence of relevant microstructural features (e.g. porosity or dispersed insulating phases) which may influence the electrical properties of a ceramic. These microstructural features can usually be detected through changes in the shape and capacitance values associated with the bulk and/or grain-boundary arcs. In some cases, the blocking effect of porosity and dispersed secondary phases may cause substantial overlap of the bulk and grain-boundary arcs.[12,13] We believe that this explanation can be used to rationalise the impedance spectra for the LSA and YSA samples under investigation in this study. The shape of the impedance spectra observed for these materials is consistent with high porosity (LSA) and the presence of an insulating secondary phase (YSA).

**Table 3.** Ionic radii and polarizabilities of cations

| | *Radius (Å)*[16] | *Polarizability ($10^{-30}$ m$^3$)*[17] |
|---|---|---|
| $La^{3+}$ | 1·36 | 1·04 |
| $Y^{3+}$ | 1·10 | 0·55 |
| $Ga^{3+}$ | 0·62 | — |
| $Al^{3+}$ | 0·535 | 0·05 |

While the low-temperature impedance spectra are strongly influenced by the presence of such microstructural features, the situation at high temperature (e.g. 800–1000°C), within the frequency range used in this work (20 Hz to 1 MHz), is completely different. In fact, it is well known that at high temperatures, impedance spectra usually consist of only a small portion of the entire spectrum (commonly only part of the electrode response), and due to stray inductance effects, cross the real axis at some intermediate frequency, e.g. $10^5$ Hz. The cross over point on the real axis corresponds closely to the total ohmic resistance of the cell. The approach used in the previous discussion was to assume that this value is closely related to the materials intrinsic behaviour. To emphasise this, the most common deviations from ideal behaviour will be briefly outlined.

For materials with relatively large grain boundary impedances (see LSG, as an example), it is common knowledge that the high temperature behaviour is controlled by the bulk response rather than by the grain boundaries, because of the high activation energy of the grain boundary conductivity. However, the presence of significant percentages of porosity (e.g. LSA), or secondary phases (e.g. the presence of garnet phase in YSA), could be extremely influential on the high temperature characteristics in two circumstances: (i) if the secondary phase was continuous and had a conductivity much higher than the dominant phase, in which case there would be an easy parallel pathway for electrical charge transport; (ii) if the insulating secondary phase (e.g. liquid along the grain boundaries) blocked all contacts between the grains of the dominant phase. Neither of these conditions were found in this work.

Porosity is certainly continuous but is insulating, and percolation of LSA grains is obvious (see Fig. 3). The garnet phase is believed to be insulating but there is also no evidence for percolation of this phase or for a systematic blocking effect (intergrain) with respect to the perovskite phase as the small perovskite grains are clearly interconnected (see Fig. 5). Thus, although all conductivity values are influenced by these poor microstructures, the role of secondary phases is only likely to influence the high temperature conductivities in a small and systematic manner. From existing knowledge on the role of insulating phases dispersed in a conductive matrix,[12,13] it has been observed that volume fractions lower than 25% only cause an apparent decrease in conductivity to one half or one third of the ideal value of a phase-pure matrix. This means that differences in conductivity of over

one order of magnitude at high temperatures, as found in this work, are unlikely to be caused by such microstructural features. The oxygen partial pressure dependence is also unaffected by the presence of these phases, for the same reasons.

One last comment on deviations from nominal composition should be made. The presence of secondary phases with significantly different composition was only observed for the chemically prepared LSA (see Fig. 4). This pellet was not used for further electrical characterisation ($\sigma$ versus $Po_2$ or ion-blocking measurements). In all other cases, and within the accuracy of the EDS analysis performed, only small deviations in Sr-content of the LSG, LSA and YSA samples were observed. Lower Sr-dopant content (with respect to the nominal composition) may explain a small abatement in ionic conductivity between the various phases due to the role of the Sr-dopant in the formation of oxygen vacancies. For a 5% dopant level, however, neither the dominant ionic defects nor the transport mechanism would suffer significantly from small deviations in Sr-content between the various samples. Although the reported conductivity values are certainly influenced by all these factors, the overall trends remain valid.

## 4 Conclusion

LSG has the highest conductivity of all the samples studied and the lowest activation energy. This material has been widely studied and the results obtained in this project are in agreement with those in the literature. Results for the LSA samples indicate that these materials have poorer conductivities and higher activation energies compared with LSG. YSA samples have the lowest conductivity of all the samples measured. Preparing single phase materials and processing dense ceramics of LSA and YSA remains a difficult and challenging problem.

High temperature electrical measurements show that different A- and B-site cations clearly influence the ionic conductivity and activation energies in these perovskite-based materials. The results in the present study contradict the trends expected from the $r_{crit}$ model and demonstrate that although cation size influences the conductivity in these materials, other factors, such as the polarisability of the ions may be more important.

## Acknowledgements

The work was partly funded by FCT (Portugal), the European Social Fund and the British Council.

## References

1. Tuller, H. L., In *Non-stoichiometric Oxides*, ed. O. Toft Sorensen. Academic Press, New York, 1981, pp. 271–335.
2. Ishihara, T, Matsuda, H. and Takita, Y., Effects of rare earth cations doped for la site on the oxide ionic conductivity of $LaGaO_3$-based perovskite type oxide. *Solid State Ionics*, 1995, **79**, 147–151.
3. Ishihara, T., Hiei, Y. and Takita, Y., Oxidative reforming of methane using solid oxide fuel cell with $LaGaO_3$-based electrolyte. *Solid State Ionics*, 1995, **79**, 371–375.
4. Ishihara, T., Matsuda, H., Azmi bin Bustam, M. and Takita, Y., Oxide ion conductivity in doped Ga based perovskite type oxide. *Solid State Ionics*, 1996, **86-88**, 197–201.
5. Ishihara, T., Matsuda, H. and Takita, Y., Doped $LaGaO_3$ perovskite type oxide as a new oxide ionic conductor. *J. Am. Chem. Soc.*, 1994, **116**, 3801–3803.
6. Huang, P-N. and Petric, A., Superior oxygen ion conductivity of lanthanum gallate doped with strontium and magnesium. *J. Electrochem. Soc.*, 1996, **143**(5), 1644–1648.
7. Takahashi, T. and Iwahara, H., Ionic conduction in perovskite-type oxide solid solution and its application to the solid electrolyte fuel cell. *Energy Conversion*, 1971, **11**, 105–111.
8. Baker, R. T., Gharbage, B. and Marques, F. M. B., Ionic and electronic conduction in fe- and cr-doped (La,Sr)-$GaO_3$. *J. Electrochem. Soc.*, 1997, **144**(9), 3130–3135.
9. Rodriguez-Carvajal, J., In *Satelite Meeting on Powder Diffraction*, abstract in the *XVth Conference of the International Union of Crystallography*. Toulouse, p. 127, 1998.
10. Kilner, J. A. and Brook, R. J., A study of oxygen ion conductivity in doped non-stoichiometric oxides. *Solid State Ionics*, 1982, **6**, 237–252.
11. Baker, R. T., Gharbage, B. and Marques, F. M. B., Processing and electrical conductivity of pure, Fe- and Cr-substituted $La_{0.9}Sr_{0.1}GaO_3$. *Journal of the European Ceramic Society*, 1998, **19**, 105–112.
12. Bernard, H., Microstructure and conductivity of sintered stabilized zirconia. Ph.D. thesis, Université Scientifique et Médicale de Grenoble-INPG, France, 1980 (in French).
13. Steil, M. C., A contribution to the study of electrical properties of heterogeneous materials (cubic zirconia based ceramics) by impedance spectroscopy. Ph.D. thesis, Ecole Nationale Superieure des Mines de Saint-Etienne, France, 1996 (in French).
14. Anderson, P., Marques, F., Sinclair, D. and West, A., Ionic and electronic conduction in $La_{0.95}Sr_{0.05}GaO_{3-\delta}$, $La_{0.95}Sr_{0.05}AlO_{3-\delta}$ and $Y_{0.95}Sr_{0.05}AlO_{3-\delta}$. *Solid State Ionics*, (in press).
15. Navarro, L. M., Marques, F. M. B. and Frade, J. R., n-Type conductivity in gadolinia doped ceria. *J. Electrochem. Soc.*, 1997, **144**(1), 267–273.
16. Shannon, R. D. and Prewitt, C. T., Effective ionic radii in oxides and fluorides. *Acta Cryst.*, 1969, **B25**, 925–945.
17. Skaarup, S., Solid electrolytes. *J. Materials Edu.*, 1984, **6**(4), 667–730.